Development 128, 4177-4188 (2001)
Printed in Great Britain © The Company of Biologists Limited 2001
DEV2743

Loss of *Eph-receptor* expression correlates with loss of cell adhesion and chondrogenic capacity in *Hoxa13* mutant limbs

H. Scott Stadler*, Kay M. Higgins and Mario R. Capecchi‡

Howard Hughes Medical Institute, University of Utah School of Medicine, Salt Lake City, UT 84112-5331, USA
*Present address: Department of Molecular and Medical Genetics, Oregon Health Sciences University and Shriners Hospital for Children, Portland, OR 97201, USA
‡Author for correspondence (e-mail: mario.capecchi@genetics.utah.edu)

Accepted 23 July 2001

SUMMARY

Mesenchymal patterning is an active process whereby genetic commands coordinate cell adhesion, sorting and condensation, and thereby direct the formation of morphological structures. In mice that lack the *Hoxa13* gene, the mesenchymal condensations that form the autopod skeletal elements are poorly resolved, resulting in missing digit, carpal and tarsal elements. In addition, mesenchymal and endothelial cell layers of the umbilical arteries (UAs) are disorganized, resulting in their stenosis and in embryonic death. To further investigate the role of *Hoxa13* in these phenotypes, we generated a loss-of-function allele in which the GFP gene was targeted into the *Hoxa13* locus. This allele allowed FACS isolation of mesenchymal cells from *Hoxa13* heterozygous and mutant homozygous limb buds. *Hoxa13^{GFP}* expressing mesenchymal cells from *Hoxa13* mutant homozygous embryos are defective in forming chondrogenic condensations in vitro. Analysis of pro-adhesion molecules in the autopod of *Hoxa13* mutants revealed a marked reduction in *EphA7* expression in affected digits, as well as in micromass cell cultures prepared from mutant mesenchymal cells. Finally, antibody blocking of the *EphA7* extracellular domain severely inhibits the capacity of *Hoxa13^{GFP}* heterozygous cells to condense and form chondrogenic nodules in vitro, which is consistent with the hypothesis that reduction in *EphA7* expression affects the capacity of *Hoxa13$^{-/-}$* mesenchymal cells to form chondrogenic condensations in vivo and in vitro. *EphA7* and *EphA4* expression were also decreased in the mesenchymal and endothelial cells that form the umbilical arteries in *Hoxa13* mutant homozygous embryos. These results suggest that an important role for *Hoxa13* during limb and UA development is to regulate genes whose products are required for mesenchymal cell adhesion, sorting and boundary formation.

Key words: Hox genes, Limb development, Ephrin receptors, Mesenchymal condensations, Mouse

INTRODUCTION

The condensation of mesenchymal cells is critical to the formation of organs and skeletal elements in vertebrates (Hall and Miyake, 1992; Hall and Miyake, 1995). In the developing limb bud, the mesenchymal condensations that give rise to the skeletal elements form from an undifferentiated mass of mesoderm derived from the progress zone. Genetic analysis has demonstrated that members of the HoxA and HoxD linkage groups are essential for this process (Dollé et al., 1993; Davis et al., 1995; Kondo and Duboule, 1999). For example, mice homozygous for a loss-of-function mutation in *Hoxa13* show major perturbations in the formation of the autopod skeletal elements and mice doubly mutant for both *Hoxa13* and *Hoxd13* fail to form autopod skeletal elements (Fromental-Ramain et al., 1996). Complementing these loss-of-function studies in mice, Yokouchi et al. (Yokouchi et al., 1995) demonstrated that misexpression of Hoxa13 in the chick proximal limb alters homophilic cell-cell interactions of mesenchyme derived from these limb buds in vitro and formation of the zeugopod skeletal elements in vivo. More recently, Wada et al. (Wada et al., 1998) identified a role for glycosylphosphatidylinositol-linked (GPI) ephrin ligands and their receptor, *EphA4*, in mediating self-sorting of undifferentiated mesenchyme into distinct proximal and distal limb skeletal structures. Hox genes belonging to the 3′-end of the HoxA and HoxB linkage groups appear to regulate expression of EphA receptors that are involved in hindbrain rhombomere boundary formation and axon guidance in this region (Taneja et al., 1996; Chen and Ruley, 1998; Dottori et al., 1998; Studer et al., 1998). These receptor genes are also expressed at high levels in the developing autopod (Ciossek et al., 1995; Flenniken et al., 1996; Wada et al., 1998). Taken together, these data suggest that EphA receptors may be targets of *Hoxa13* and provide a molecular mechanism for how boundaries may be established during the formation of autopod mesenchymal condensations, as well as during the formation of the umbilical arteries (UAs). To test this hypothesis, we have examined how loss of Hoxa13 function affects patterning of the mesenchyme in the autopod and UAs, and specifically how EphA ligand/receptor expression and function are affected by this mutation.

MATERIALS AND METHODS

Vector construction

The *Hoxa13* replacement vector was constructed from 10 kb *Sph*I-*Eco*RI genomic fragment containing the *Hoxa13* locus. The *GFP loxP* neo cassette (Godwin et al., 1998) was cloned into a unique *Eco*RV site located in the second exon of *Hoxa13*. Continuity of the reading frame across the *Hoxa13*/GFP junction was verified by DNA sequencing. Finally the herpes simplex virus thymidine kinase gene was inserted 3′ of the *Hoxa13* genomic fragment for negative selection (Mansour et al., 1988).

Generation of targeted ES cell lines and germline transmitting mice

The targeting vector was electroporated into R1 embryonic stem cells (Nagy et al., 1993) and the cells subjected to positive and negative selection (Mansour et al., 1988). Genomic DNA from 144 colonies was digested with *Sph*I and analyzed by Southern transfer analysis to identify two homologous recombinants. Cells from both recombinant clones were microinjected into C57BL/6 blastocysts to generate chimeric mice. Chimeric males were crossed to C57BL/6 females and DNA from Agouti progeny was tested by Southern blotting and PCR analysis to confirm germline transmission of the mutant *Hoxa13*^{GFPneo} allele (Fig. 1C). Embryos from heterozygous intercrosses were genotyped by PCR using yolk-sac DNA. PCR conditions consisted of 35 cycles of 94°C for 15 seconds, 62°C for 15 seconds and 72°C for 35 seconds. Mutant (378 bp) and wild-type (177 bp) amplification products (Fig. 1D) were produced using the *Hoxa13* forward primer (GTCGTCTCCCATCCTTCAGAC), the GFP reverse primer (GCACTGCACGCCGTAGGTCA) and the *Hoxa13* reverse primer (TGTTCTGGAACCAGATTGTGAC; Fig. 1B). The neomycin resistance cassette was removed by crossing *Hoxa13*^{GFP} heterozygous females to *Cre* deleter mice (Schwenk et al., 1995).

Fluorescent imaging

Embryos derived from heterozygous intercrosses were harvested at gestational ages ranging from embryonic day (E) 9.5 to 15.5 and placed in Leibovitz's L-15 media lacking Phenol Red (Gibco/BRL). Imaging of dissected limbs, tissue culture samples and intact embryos used either Sylgard plates or depression slides, depending on sample size. GFP, CY5, TO-PRO-3 and Texas red fluorescence were recorded using a BioRad MRC 1024 laser scanning confocal imaging system fitted to a Leitz Aristoplan microscope using filters supplied by the manufacturer. A digital Kalman averaging filter was used with the GFP and Texas Red fluorescence to reduce background fluorescence.

Micromass cultures

Staged limb buds (Wanek et al., 1989) from mutant and heterozygous embryos at gestational age E11.5 were collected in 4°C Ca^{2+}- and Mg^{2+}-free phosphate-buffered saline (PBS; Gibco/BRL). Enrichment for *Hoxa13*^{GFP} expressing cells was achieved either by microdissection of the fluorescent regions of the limb bud using fine tungsten needles and a fluorescence equipped Leica MZ12 stereoscope or by cell sorting using a Becton Dickinson FACS ADVANTAGE cell sorter. The two enrichment methods produced similar results. Dissected tissues were dissociated at 37°C for 10 minutes in Ca^{2+}- and Mg^{2+}-free PBS (Gibco/BRL) containing 0.1% trypsin and 0.1% collagenase as described (Owens and Solursh, 1982), followed by pipetting three to five times through a sterile 70 μm cell basket (Costar). The cell suspension was washed twice using 5 ml of serum free Dulbecco's MEM media (Gibco/BRL) and counted on a hemocytometer. The cell suspensions were diluted to a final concentration of 2×10^7 cells/ml with Dulbecco's MEM media containing 15% FBS supplemented with non-essential amino acids, 50 U/ml penicillin and 25 ug/ml streptomycin. Cell suspensions were inoculated onto 60 mm Falcon tissue culture dishes as described (Ahrens et al., 1977) and placed in a 37°C incubator with a 6% CO_2 atmosphere for 1 hour to allow for cell attachment. After 1 hour the plates were flooded with 8 ml of media which was changed daily. Mesenchyme aggregations were recorded 19 hours after plate inoculations, whereas cartilaginous nodules were analyzed 3-4 days later.

Antibody blocking assay

Hoxa13^{GFP}-expressing tissues from the autopods of E12.5 embryos were dissected and dissociated with 0.05% trypsin-EDTA and 0.05% collagenase followed by passage through 70 μm Netwell filters (Costar) to generate single-cell suspensions. The single cell suspensions were plated at a density of 2×10^7 cells/ml in 20 μl aliquots in 60 mm tissue culture dishes. A second 20 μl aliquot containing either 4 μg of a rabbit EphA7 polyclonal antibody dialyzed for 4 hours in 1× PBS (Santa Cruz Biotechnology Cat. No. SC-917), pre-immune rabbit serum, or DMEM media was immediately added to the micromass cells which were then incubated at 37°C for 1 hour. After incubation, 7 ml of DMEM media supplemented with 10% fetal calf serum and 50 U/ml penicillin, and 25 μg/ml streptomycin was added to each dish. A second aliquot of the EphA7 antibody, or rabbit serum was added to the respective dishes in conjunction with the 7 ml of media. The cells were grown in a standard 37°C incubator at 5% CO_2. Micromass cultures were photographed 48 hours after plating under phase contrast using a Leica DMIL microscope fitted with a Nikon Coolpix 990 digital camera.

Cell sorting assay

Proximal limb bud tissues (400-500 μm from the AER) from stage matched E11.5 Swiss Webster embryos were dissected and processed for micromass culture as described above. At the same time, the fluorescent regions of stage matched E11.5 limb buds from *Hoxa13*^{GFP} mutant and heterozygous embryos were dissected and processed for micromass culture. Stock suspensions of wild-type Swiss Webster cells, *Hoxa13*^{GFP} mutant cells and heterozygous cells were adjusted to equivalent concentrations of 4×10^7 cells/ml. From these stock suspensions, micromass plates were inoculated with equal concentrations of wild-type and either mutant or heterozygous cells as described (Ahrens et al., 1977; Owens and Solursh, 1982; Ide et al., 1994). Nineteen hours after inoculation, the attached cells were stained with TO-PRO-3 iodide (Molecular Probes) and analyzed for proximal-distal sorting of wild-type and *Hoxa13*^{GFP}-expressing cells using the previously described BioRad Confocal Imaging System.

Immunohistochemistry

E11.5 limbs were fixed at room temperature in Carnoy's fixative for 2 hours followed by rinses in 1× PBS containing 0.5% Triton X-100 (PBX) for an additional 2 hours. Tissues were then placed in a PBX blocking solution containing 4% skim milk and 2% donkey serum, and rocked slowly at 4°C for 4 hours. NCAM (5B8) and collagen type II (II-II6B3) mouse antibodies (Developmental Hybridoma Bank, University of Iowa, Iowa City, IA) were diluted in PBX containing 2% skim milk and 2% donkey serum, and incubated with the limb tissue overnight at 4°C. The primary antibody was removed and the limbs were washed for 3 hours in PBX at room temperature. After washing, the limbs were incubated overnight at 4°C with a donkey anti-mouse secondary antibody conjugated with either Texas Red or Cy5 (Jackson Immunological). Confocal analysis was performed as described above.

For micromass cultures, the media was removed and the anchored cells were washed briefly in 1× PBS followed by fixation in 4% formaldehyde for 10 minutes. After fixing, the cells were again rinsed in 1× PBS for 20 minutes, followed by permeabilization and blocking in PBX containing 2% skim milk and 2% donkey serum for 1 hour. After blocking, primary antibodies, including EphA2, EphA4 and EphA7 (Santa Cruz Biotechnology), ephrin A1, ephrin A2 and ephrin A3 (Santa Cruz Biotechnology), N-Cadherin (Transduction Labs), β-catenin (Transduction Labs), Paxillin (Transduction Labs), E-Cadherin

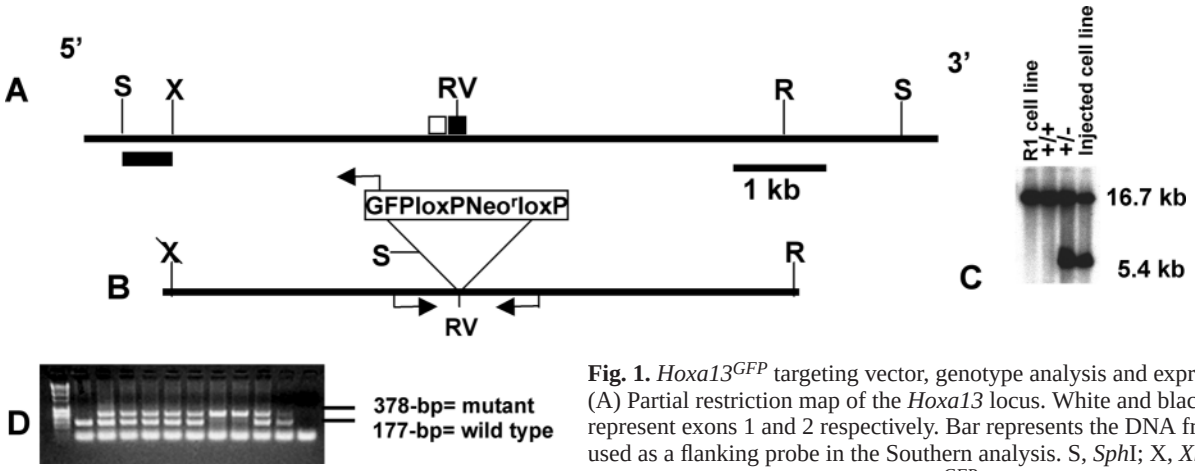

Fig. 1. *Hoxa13*^{GFP} targeting vector, genotype analysis and expression. (A) Partial restriction map of the *Hoxa13* locus. White and black boxes represent exons 1 and 2 respectively. Bar represents the DNA fragment used as a flanking probe in the Southern analysis. S, *Sph*I; X, *Xho*I; RV, *Eco*RV; R, *Eco*RI. (B) 10 kb *Hoxa13*^{GFP} targeting vector. Forward and reverse PCR primer sites are denoted by the black arrows. (C) Southern transfer analysis of homologous recombinants and germline transmission with *Sph*I DNA digested from wild-type Agouti offspring (+/+), and Agouti offspring showing germline transmission of the *Hoxa13*^{GFP} allele (+/–). (D) PCR genotyping of embryonic yolk-sac DNAs derived from a heterozygous intercross.

(Transduction Labs), antiphosphohistone H3 (Upstate Biotechnology), and D1C4 (a kind gift from Anthony Capehart), were incubated with the micromass cultures in blocking solution overnight at 4°C. The next day, the primary antibody was removed, and the micromass cultures were washed for 3 hours at room temperature in 1× PBS, followed by an overnight incubation at 4°C in blocking solution with a species specific Cy5-conjugated donkey secondary antibody.

For cryosections, embryos were fixed for 2 hours in 4% paraformaldehyde and briefly rinsed in 1× PBS for 10 minutes. Cryoprotection of the embryos was achieved using a sequential series of 10, 20 and 30% sucrose/PBS solutions. The embryos were oriented in OCT (Tissue Tek) filled molds and rapidly frozen. The embryos were sectioned on a Zeiss Cryostat at a thickness of 20-30 μm. Sections were mounted on Superfrost plus slides (Fisher) for microscopic and immunohistochemical analysis.

RNA in situ hybridization

Plasmids containing the EphA7 (Mdk1) and Msx1 genes generously provided by Drs T. Mori and Y. Chen, respectively, were used to produce antisense riboprobes. Embryo preparation, hybridization and analysis were performed as previously described (Manley and Capecchi, 1995). BM-Purple (BMB-Roche) was used for the alkaline phosphatase color reactions, which were extended for 17 hours at room temperature for the EphA7 riboprobe.

TUNEL analysis of apoptosis

Terminal UTP nick end labeling (TUNEL) of DNA was performed as a modification of the technique described by Maden et al. (Maden et al., 1997). Limbs from E11.5-13.5 embryos were fixed at room temperature for 2 hours in 4% paraformaldehyde. After fixing, the limbs were washed for 3 hours at room temperature with several changes of 1× PBS containing 1% TritonX-100. The limbs were placed in 1.5 ml microfuge tubes and pre-incubated at 37°C for 30 minutes in PBS containing 1× terminal transferase buffer (Boehringer Mannheim Biochemical), 1% Triton X-100 and 2.5 mM $CoCl_2$. The preincubation buffer was replaced with a 1× PBS solution containing 1× terminal transferase buffer, 10 μM dUTP (2:1 dUTP:dUTP-biotin), 2.5 mM $CoCl_2$, 1% Triton X-100 and 0.5 U terminal transferase/μl buffer, and incubated at 37°C for 3 hours. The limbs were then washed for 3 hours in PBS and incubated overnight at 4°C with streptavidin conjugated with Texas Red (Jackson Immunological). After washing for 1 hour in PBS, confocal analysis of the limbs was performed as described above.

RESULTS

Generation of the Hoxa13^{GFP} mutant allele

The loss-of-function allele, *Hoxa13*^{GFPneo}, was targeted into the *Hoxa13* locus of mouse ES cells by homologous recombination (Capecchi, 1994; Fig. 1A-D). The floxed neomycin resistance cassette was removed from the germline of animals generated from these ES cells by breeding to a *Cre*- deleter mouse (Schwenk et al., 1995), generating mice with the *Hoxa13*^{GFP} allele. Mice carrying either *Hoxa13* mutant allele showed similar phenotypes in heterozygous and homozygous form. The studies reported herein predominantly used mice and embryos carrying the *Hoxa13*^{GFP} allele.

Hoxa13^{GFP} expression was characterized in E10.5-E13.5 embryos to confirm accurate recapitulation of the published *Hoxa13* mRNA expression pattern (Haack and Gruss, 1993; Warot et al., 1997). As early as E10.5, strong expression can be seen in the distal forelimb mesenchyme, but not in the overlying apical ectodermal ridge (AER) (Fig. 2A). By E 11.5, *Hoxa13*^{GFP} expression is readily detected in the progress zone (Fig. 2B) of the elongating limb bud. By E13.5 limb expression of *Hoxa13*^{GFP} appears to be restricted to the condensing digit mesenchyme, at the sites where many of the chondrogenic defects occur in *Hoxa13* homozygous mutant mice (Fig. 2C,D; Fromental-Ramain et al., 1996). Finally, the GFP-tagged allele of *Hoxa13* identifies the population of mesenchymal cells expressing *Hoxa13* in the developing umbilical arteries (Fig. 2E,G,H) and genitourinary regions, including the genital ridge and tissues surrounding the urogenital sinus (Fig. 2F). Our *Hoxa13*^{GFP}-null homozygotes die in utero between E11.5 and E15.5, exhibiting limb and umbilical vascular defects similar to those in mice homozygous for the *Hoxa13* mutant alleles as described previously (Fromenthal-Ramain et al., 1996; Warot et al., 1997). Examination of umbilical arteries from homozygous mutants (Fig. 2H) revealed nearly a complete loss of mesenchymal/endothelial cell layer stratification relative to heterozygous littermate controls (Fig. 2G).

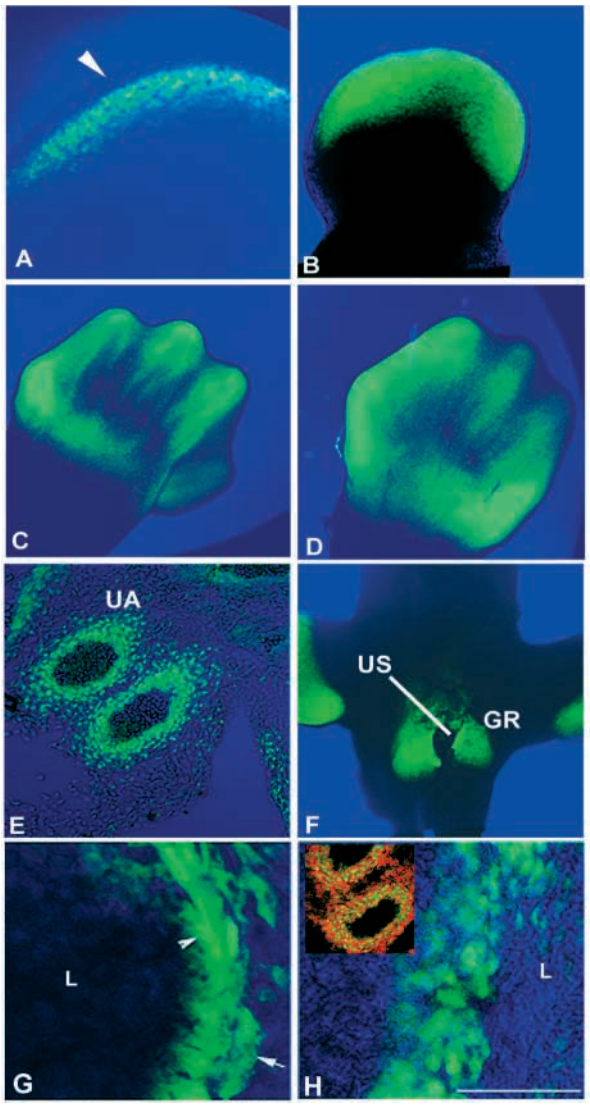

Fig. 2. Expression characterization of Hoxa13^{GFP} allele in the heterozygous embryos. (A) Expression in the distal forelimb at E 10.5. Arrowhead denotes no expression in the AER. (B) Hoxa13^{GFP} expression expands within the progress zone at E11.5. Localization of Hoxa13^{GFP}-expressing cells to the condensing digit regions in E 13.5 forelimbs (C) and hindlimbs (D). (E) Condensing vascular mesenchyme in the umbilical arteries (UA) also expresses Hoxa13. (F) Expression of Hoxa13^{GFP} is also readily detected in the genital ridge (GR) and tissues surrounding the urogenital sinus (US). (G) Higher magnification image of E 11.5 heterozygous umbilical artery showing Hoxa13^{GFP} expression in the condensing mesenchymal (arrow) and endothelial (arrowhead) layers. Vascular lumen (L). (H) Higher magnification image of an E11.5 homozygous mutant UA showing a lack of mesenchymal/endothelial cell layer stratification. Inset is the normal expression of ephrin A3 in a mutant umbilical artery demonstrating that the lack of stratification does not globally affect gene expression patterns. L, vascular lumen. Scale bar: 50 μm for G,H.

Hoxa13 is required for normal mesenchymal cell attachment and condensation

Enriched populations (~95% purity) *of Hoxa13^{GFP}*-expressing mesenchymal cells, either heterozygous or homozygous for the *Hoxa13^{GFP}* mutation, were isolated by FACS (see Materials and Methods) from E11.5-E12.5 limb buds. These cells were compared in vitro for phenotypes attributable to the loss of *Hoxa13* function. The first property examined was their ability to form condensations in culture, using the mass culture assay developed by Solursh and colleagues. This assay accurately recapitulates prechondrogenic and chondrogenic events associated with normal limb development (Ahrens et al., 1977; Owens and Solursh, 1982).

Although care was taken to plate identical numbers of *Hoxa13^{GFP}* heterozygous and homozygous mutant cells, it is apparent that after 12 hours in culture, fewer mutant homozygous cells adhere to the culture dish and initiate aggregation, compared with *Hoxa13^{GPF}* heterozygous cells (Fig. 3A,B). Eighteen to 24 hours after plating, the *Hoxa13* heterozygous mesenchymal cells aggregate into multiple dense precartilaginous condensations (Fig. 3C). Seventy-two hours later, these aggregates differentiate into cartilaginous nodules (Fig. 3I) that stain positively with Alcian Blue (Fig. 3I, inset) and express collagen type II (Fig. 3J). With further in vitro culture, the *Hoxa13*-expressing cells become restricted to the periphery of the condensate, forming digit-like structures (Fig. 3K). This restriction in *Hoxa13^{GFP}* expression to the periphery of the digit-like elements in vitro is noteworthy, because during the later stages of normal chondrogenesis in the developing limb bud, 5′-Hox gene expression becomes restricted to the perichondrium, a layer of cells that surrounds each condensate and controls its pattern of growth (Davis and Capecchi, 1994). The same sequence of differentiation is observed with unsorted mesenchymal cells isolated from wild-type embryonic limbs. However, approximately 24 hours of additional culture time is needed with the wild-type, unsorted mesenchymal cells isolated from limb buds to reach the equivalent state of differentiation. The precocious behavior of the *Hoxa13^{GFP}* heterozygous cells relative to wild-type cells may be due to the former cells being a more purified and distinct (i.e. FACS-purified and *Hoxa13*-expressing) population of mesenchymal cells.

In sharp contrast to either *Hoxa13^{GFP}* heterozygous or wild-type mesenchymal cells derived from embryonic autopods, *Hoxa13^{GFP}* mutant homozygous mesenchymal cells form fewer precartilaginous aggregates (i.e. approximately eightfold less), and those that do form are often smaller and less robust than those prepared from control mesenchyme (Fig. 3D).

To determine whether *Hoxa13* homozygous mutant cells can participate in the production of condensates in the presence of wild-type cells, equal numbers of dissociated wild-type cells (GFP negative) and homozygous mutant cells (GFP positive) were combined and plated onto culture dishes. The combined cells produced large mesenchymal condensates containing fluorescent (–/–) and nonfluorescent (+/+) cells (Fig. 3E,F). Examination of these mixed aggregates revealed that the mutant (–/–) cells contributed to the condensing mesenchyme by attaching to anchored wild-type cells (Fig. 3G,H). Both mutant and wild-type cells within these aggregates subsequently express collagen II. Thus, in the presence of wild-type cells, *Hoxa13$^{-/-}$* cells are capable of forming aggregates and differentiating along the chondrogenic pathway. This suggests that a major deficit of *Hoxa13$^{-/-}$* mesenchymal cells is in their inability to self-aggregate and adhere to the culture dish.

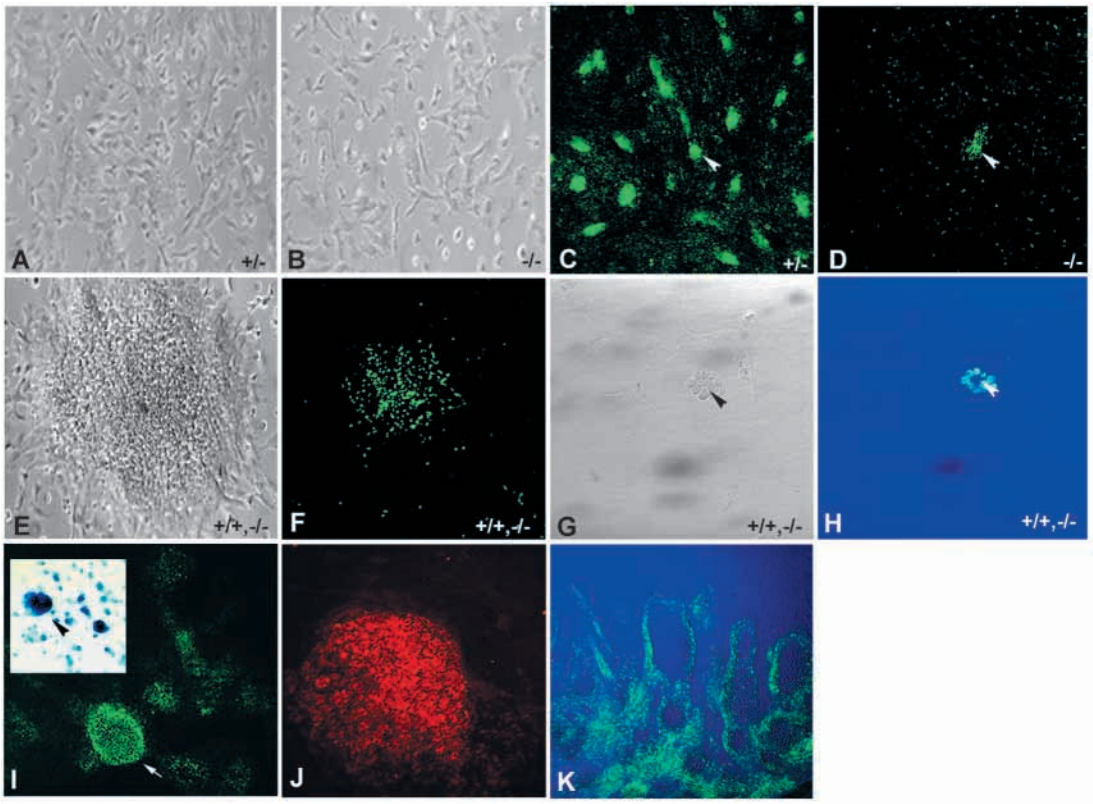

Fig. 3. In vitro analysis of cell attachment and aggregation of dissociated limb mesenchyme. FACS-enriched *Hoxa13* mutant homozygous cells demonstrated marked reduction in cell adhesion and mesenchymal aggregate formation compared with sorted cells from heterozygous littermates. (A,B) Heterozygous and homozygous mutant cultures 12 hours after plating. Although unattached to the plates, the homozygous mutant cells appeared viable as measured by Trypan Blue exclusion (data not shown). (C) Aggregation of heterozygous mutant cells in the developing mesenchymal aggregates (arrowhead) 24 hours after plating. (D) Homozygous mutant cultures typically exhibited an approximate eightfold reduction in cell attachment and mesenchyme aggregate (arrowhead) formation. (E,F) Combined mutant (–/–) and wild-type (+/+) cells demonstrate that *Hoxa13*^{GFP} –/– cells will aggregate efficiently in the presence of wild-type (GFP nonexpressing) cells, forming a large chimeric aggregate. (G,H) Higher magnification reveals that homozygous mutant mesenchymal cells contribute to chimeric mesenchyme aggregation by binding to wild-type cells, which attach more efficiently to the tissue culture dish. Arrowheads indicate the position of an attached wild-type (non-fluorescent) cell. (I) Hoxa13^{GFP} +/– cells contributing to a developing cartilage nodule 72 hours after plating (arrow). Inset shows positive staining of the nodules for Alcian Blue (arrowhead) and collagen type II (J). (K) Micromass culture of FACS-enriched Hoxa13^{GFP} +/– cells 6 days after plating, demonstrating the capacity to form digit-like structures in vitro.

Hoxa13 function correlates with *EphA7* expression in the limb mesenchyme

In homozygous mutant and wild-type limbs, no quantitative differences in the expression of the following cell surface and pro-adhesion molecules were detected at E11.5-E13.5: paxillin, β-Catenin, E-cadherin, EphA2, EphA4, ephrin A1, ephrin A2, D1C4, desmoglein, NCAM, fibronectin, catenin, collagen Type II and integrin B1 (data not shown).

In E13.5 limbs, *EphA7* mRNA is localized to the condensing digit and carpal/tarsal mesenchyme (Fig. 4A-D). In mutant fore- and hindlimbs, levels of *EphA7* expression were consistently lower in all digits, with even lower levels of expression in the regions where digit I and digit V are derived. In the forelimb, an additional region of *EphA7* expression was also present in the dorsalmost aspect of each digit, delineating the region where tendons differentiate (Fig. 4A). However, in mutant forelimbs, only digit II appeared to demonstrate *EphA7* expression in the dorsal tendon region (Fig. 4B).

The reduction of *EphA7* expression is also apparent from immunohistochemical analysis of frozen sections of mutant versus control autopods (Fig. 4E-J). Interestingly, the very low level of *EphA7* expression in the mutant autopods is not restricted to the mesenchyme, where *Hoxa13* is normally expressed, but is also observed in the overlying epidermis. From analysis of these sections, it is apparent that the mesenchyme in the mutant homozygotes is disorganized and that the boundaries between the mesoderm and epidermis are poorly defined. We consistently observe that the epidermis in these mutant animals is thicker than normal and distorted (Fig. 4L). By contrast, the distal digit mesenchyme in age-matched heterozygous controls forms a distinct boundary of *Hoxa13*^{GFP}-expressing cells immediately adjacent to the overlying epidermis (Fig. 4K). Mesenchyme condensations also appear more organized in heterozygous digits, forming proximal to the boundary layer of *Hoxa13*^{GFP}-expressing cells (Fig. 4E-H).

Consistent with the above observations, the marked reduction in *EphA7* expression is also observed in vitro, comparing micromass mesenchymal cultures prepared from mutant homozygous and heterozygous control embryonic autopods (Fig. 4M-P).

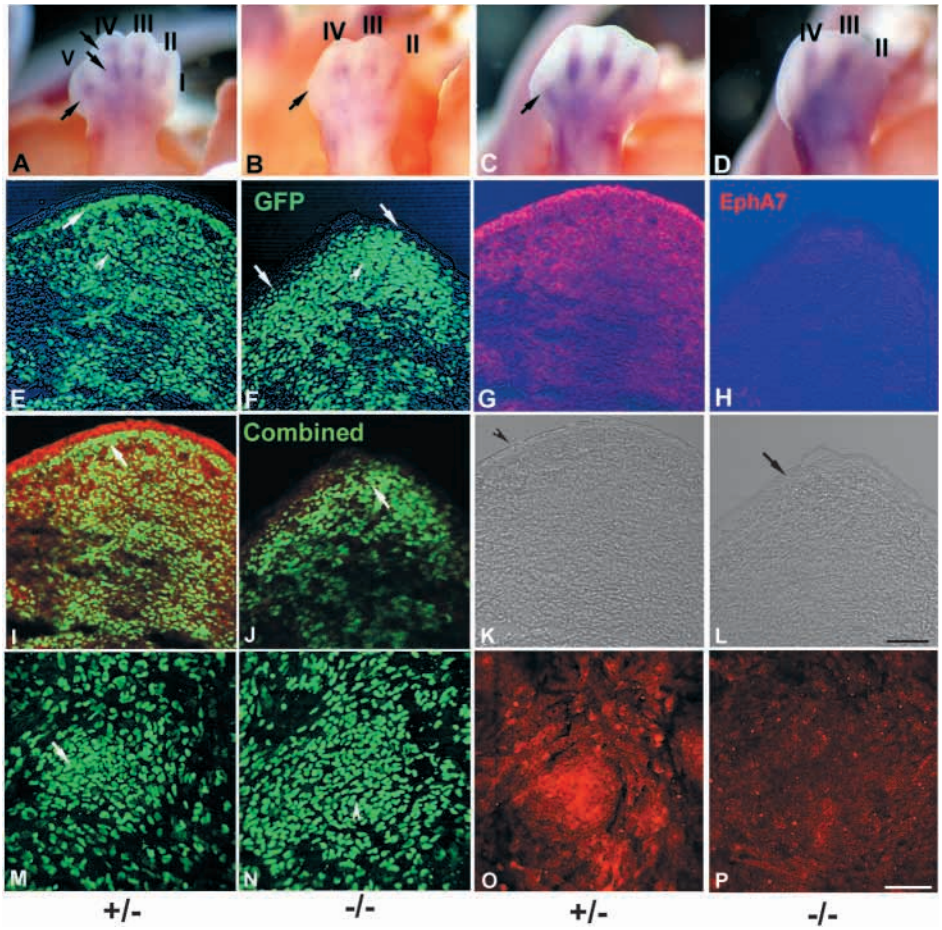

Fig. 4. Expression of EphA7 in E 13.5 limbs and micromass cultures as detected by in situ hybridization and immunohistochemistry. (A) Heterozygous mutant left forelimb. Arrows denote EphA7 expression in phalangeal condensations P1 and P2 for digit IV and the condensing digit V mesenchyme. (B) Homozygous mutant left forelimb. Arrow denotes the presumptive digit V region. (C) Heterozygous mutant left hindlimb. Arrow denotes expression in the digit V region. (D) EphA7 expression in the hindlimb of a homozygous mutant littermate. (E) Hoxa13^{GFP} expression in the distal P2 anlage of digit II in heterozygous forelimbs. Arrow denotes localization of Hoxa13^{GFP}-expressing mesenchyme to the mesodermal/epidermal boundary. Arrowhead denotes the position of mesenchymal condensation proximal to the epithelial/mesodermal boundary. (F) Localization of mesenchyme expressing Hoxa13^{GFP} in a mutant digit II anlage. Arrows denote mesenchymal cells present in the epidermal layer. Arrowhead indicates the distally shifted mesenchymal condensation of the mutant digit anlage. (G) EphA7 expression in the mesodermal and epidermal layers of the same heterozygous digit II region. (H) Reduced EphA7 expression in the same mutant digit II region. (I) Combined image of Hoxa13^{GFP} and EphA7 in the same heterozygous digit II section. Arrow indicates the precise delineation of the boundary separating mesodermal cells expressing Hoxa13^{GFP} from the overlying epidermis that expresses EphA7. (J) Combined expression of Hoxa13^{GFP} and EphA7 in the same mutant digit II region. Note the complete absence of a defined mesodermal/epidermal boundary, as well the more distal localization of the condensing digit mesenchyme (arrow). (K) Bright-field image of the same heterozygous digit II region. Note the thin uniformly defined layer of cells comprising the epidermal layer (arrowhead). (L) Bright field image of the same mutant digit II region. Note the thickened, irregularly shaped epidermal layer (arrow). (M) Aggregating limb mesenchyme expressing Hoxa13^{GFP} isolated from limb buds heterozygous for the *Hoxa13* mutation. Note the dense configuration of cells forming the central mesenchymal condensation (arrow). (N) Aggregating limb mesenchyme isolated from limb buds homozygous for the *Hoxa13* mutation. Note the reduced cell density in mesenchymal condensations derived from homozygous mutant cells (arrowhead). (O) EphA7 is highly expressed in mesenchymal condensations prepared from cells heterozygous for the *Hoxa13* mutation. (P) EphA7 expression is missing in condensations prepared from mesenchyme homozygous for the *Hoxa13* mutation. Scale bars: 100 μm for E-L; 50 μm for M-P.

Ephrin A3 expression is altered in *Hoxa13^{GFP}* mutant limbs

The distribution of the ephrin ligand A3, which binds with high affinity to the *EphA7* receptor (Janis et al., 1999), was examined in the developing autopod of homozygous Hoxa13^{GFP} mutant and heterozygous embryos. By E13.5 the expression of *ephrin A3* and *Hoxa13^{GFP}* in heterozygotes is restricted to the perichondrial region (Fig. 5A,C,E). However, in mutant limbs, this perichondrial restriction is not apparent, as both *HoxaA13^{GFP}* and *ephrin A3* are expressed throughout the developing digit and interdigit regions (Fig. 5B,D,F). Notably, the cells contributing to the digit condensations were discernable in the mutant limb sections under bright field microcopy (Fig. 5G,H), and the cells defining the perichondrial boundary were not visible, suggesting that *Hoxa13* is involved in establishing the boundary between the perichondrium and the adjacent condensing mesenchyme.

In vitro condensations of autopod mesenchyme can be blocked with an anti-*EphA7* antibody

A blocking antibody specific for the extracellular domain of *EphA7* was used to correlate how reductions in *EphA7* expression may contribute to the changes in cell adhesion and mesenchymal condensation exhibited by *Hoxa13^{GFP}* mutant (–/–) mesenchymal cells. Incubations of heterozygous (+/–) limb mesenchymal cells with either pre-immune rabbit sera or DMEM media, had no affect on the capacity of these cells to adhere and aggregate into chondrogenic nodules in vitro (Fig. 6A,B,D,E). By contrast, the addition of the anti-*EphA7* antibody dramatically reduced both cell adhesion and chondrogenic nodule formation of Hoxa13^{GFP} heterozygous cells. This reduction in cell adhesion and aggregate formation in the antibody treated samples of heterozygous cells closely resembles the aggregation and cell adhesion efficiencies of Hoxa13^{GFP} mutant (–/–) cells, which, because of their low levels

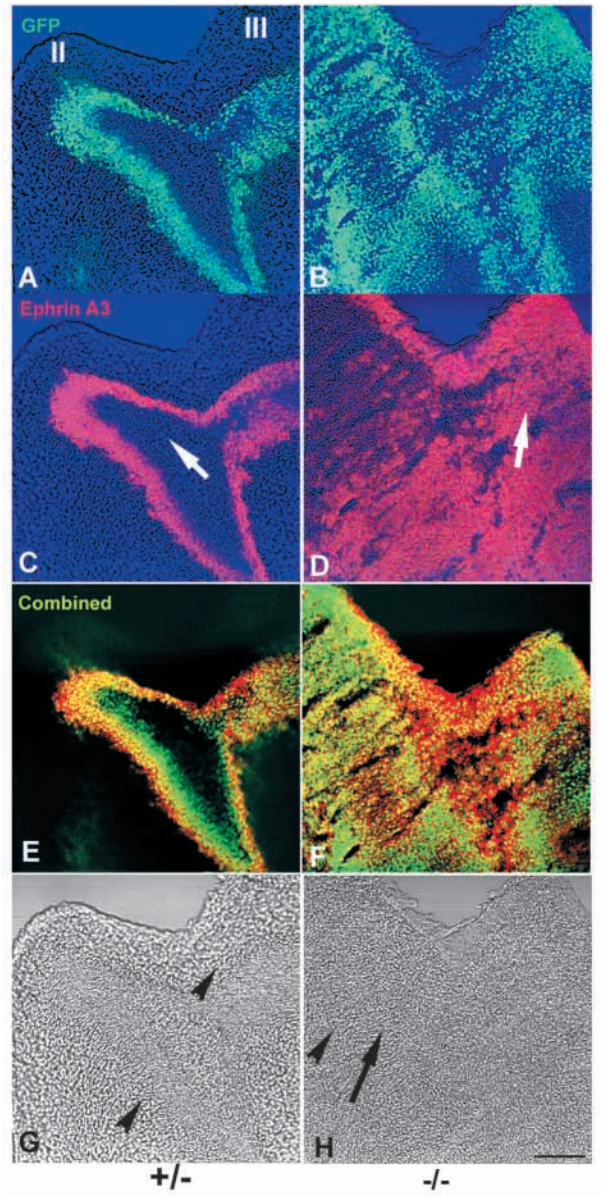

Fig. 5. Ephrin A3 expression in the developing autopod of Hoxa13^{GFP} mutant homozygous and heterozygous littermates at E 13.5. (A) Perichondrial expression of Hoxa13^{GFP} in digits II and III in a heterozygous limb section. (B) Expression of Hoxa13^{GFP} in a mutant littermate section, showing decreased maturation of the digit anlage as well as poor delineation of the perichondrial border. (C) Expression of ephrin A3 in the developing digit II and III perichondrial borders of the same heterozygous limb section. Note the lack of ephrin A3 expression within the condensing digit anlage (arrow). (D) Diffuse expression of ephrin A3 in the same mutant limb section reflecting the undifferentiated status of the digit mesenchyme. Arrow denotes the site of a poorly delineated digit II perichondrium. (E) Co-localization of Hoxa13^{GFP} expressing mesenchyme and ephrin A3 in the perichondrium of the developing heterozygous digit anlage. Note that the strong delineation of the outermost portion of the perichondrial border is demarcated by the highest levels of Hoxa13^{GFP} and ephrin A3 expression (yellow cells). (F) Co-localization of Hoxa13^{GFP} and ephrin A3 in the mutant digit II-III region. Noticeably absent are yellow cells depicting the delineation of the outer perichondrial border. (G) Bright field image of the condensing digit mesenchyme and perichondrial border in the same heterozygous section. Note the clear demarcation of the perichondrial border (arrowheads) from the condensing digit II and III mesenchyme (arrows). (H) Bright field image of the same mutant limb section. Note the poor separation between the putative perichondrial region (arrowhead) and the condensing digit anlage (arrow). Scale bar: 100 μm.

of *EphA7* expression, were unaffected by the blocking antibody (compare Fig. 6G,H with 6C,F,I).

Positional cell sorting is altered in the autopod of *Hoxa13*^{GFP} embryos

Because EphA receptors and their ligands may regulate mesenchymal cell sorting along the proximal-distal axis of the autopod (Wada et al., 1998), we asked whether the loss of *Hoxa13* affects the ability of distal cells to sort themselves in vitro from condensates formed from more proximal wild-type mesenchyme. In micromass cell cultures prepared from equal numbers of dissociated mesenchymal cells of distal, *Hoxa13*^{GFP} heterozygous cells (green) and more proximal wild-type cells, the GFP-labeled cells formed tight aggregates that excluded wild-type cells (Fig. 7A,C,E). By contrast, in similar aggregates prepared from mixtures of wild-type cells and *Hoxa13*^{GFP} mutant homozygous cells, the GFP-labeled cells were not able to sort themselves from the wild-type cell aggregates (Fig. 7B,D,F).

Interdigital tissue persists in *Hoxa13* heterozygous and mutant homozygous mice

In 37% of adult *Hoxa13*^{GFP} heterozygotes (n=106) there are soft tissue fusions between hindlimb digits II and III (Fig. 8A,B). In mutant homozygotes, no interdigital separation was apparent between any of the forelimb or hindlimb digits of living embryos at stages E13.5 and E14.5 (data not shown). TUNEL assays for apoptosis in E13.5 heterozygous and mutant homozygous embryos revealed reduced and undetectable levels of apoptosis between digit II and III of *Hoxa13*^{GFP} mutant heterozygous and homozygous embryos, respectively, compared with wild-type controls (Fig. 8D-F). Confocal microscopic examination of sectioned hindlimb tissues revealed the ectopic presence of *Hoxa13*^{GFP}-expressing cells in the interdigital region of *Hoxa13*^{GFP} heterozygous and homozygous animals, respectively (Fig. 8G,H). The presence of ectopic *Hoxa13*^{GFP} expressing cells in the interdigital region of the mutant embryos is suggestive of a failure in cell sorting and maintenance of appropriate cellular boundaries.

Detection of normal expression levels of Msx-1 in the mutant limb interdigital tissues (Fig. 8K,L) suggests that the loss of programmed cell death (PCD) in these tissues is not the result of delayed growth and development. More likely, the loss of PCD in Hoxa13^{GFP} mutant limbs reflects changes in either the capacity of these tissues to respond to apoptotic signals or in the levels of pro-apoptotic factors required for interdigital PCD.

Hoxa13 is necessary for *EphA7* and *EphA4* expression in condensing vascular mesenchyme

Hoxa13^{GFP} homozygous mutant embryos demonstrate a consistent narrowing of the umbilical arteries as early as E10.5, with complete ablation of the lumen of one of the vessels occurring by E13.5 in all (4/4) mutant embryos examined (data not shown). Confocal microscopy of sections containing the

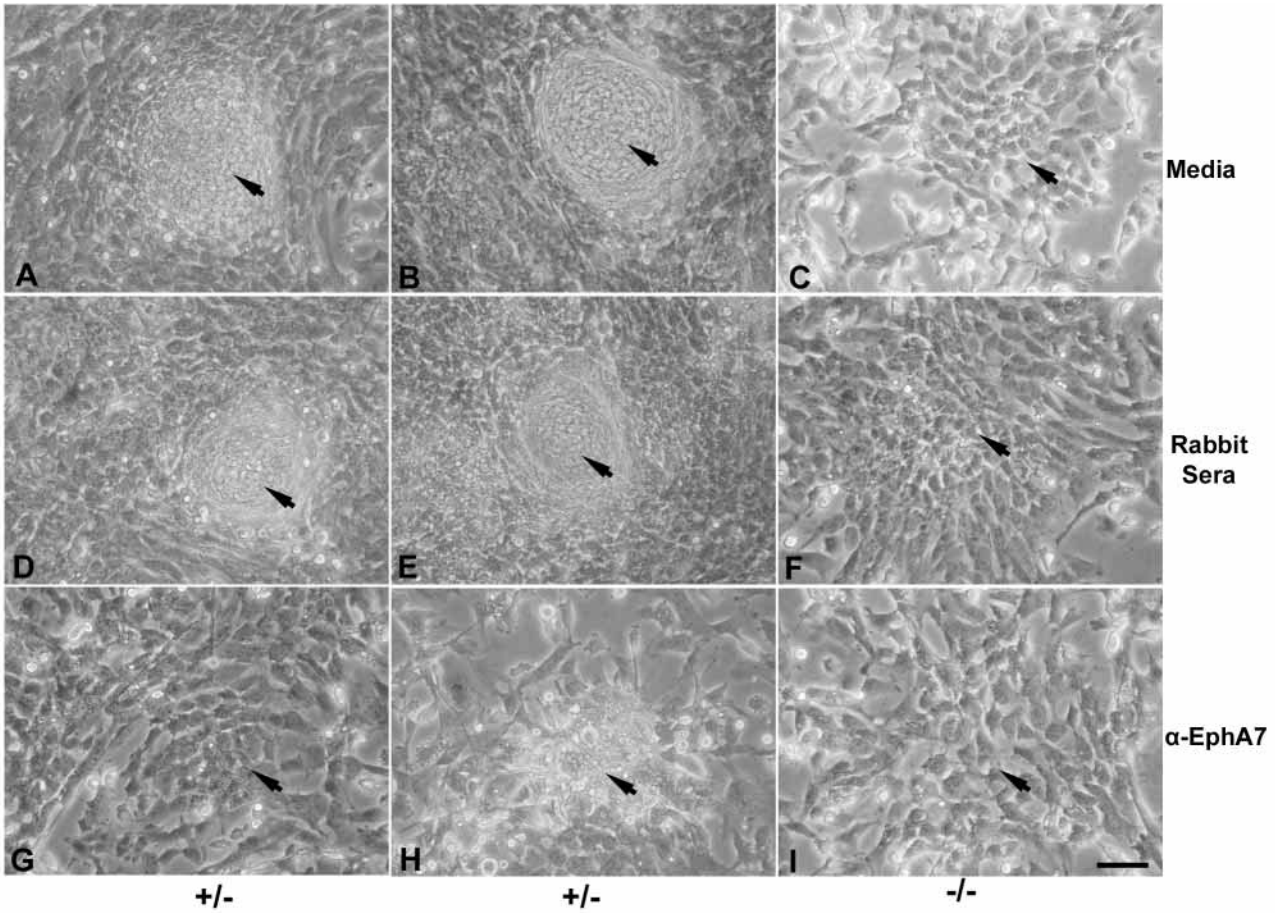

Fig. 6. In vitro application of an EphA7 antibody disrupts mesenchyme aggregation and chondrogenic nodule formation. (A,B) Micromass cultures of E 12.5 Hoxa13^{GFP} heterozygous (+/–) mesenchymal cells 48 hours after incubation with DMEM media. Arrows denote normal aggregation and development of chondrogenic nodules. (C) Micromass culture of an E12.5 Hoxa13^{GFP} homozygous mutant (–/–) limb mesenchyme plated at the same cell density as (A,B) and treated with DMEM media. Arrow denotes minimal cell aggregation and condensation. (D,E) Parallel cultures of E 12.5 Hoxa13^{GFP} (+/–) mesenchymal cells 48 hours after incubation with normal rabbit serum, indicating that serum lacking EphA7 antibodies had no effect on the capacity of the heterozygous mesenchyme to aggregate and form chondrogenic nodules (arrows). (F) Homozygous mutant mesenchyme is also unaffected by incubation with the rabbit serum as minimal condensations are still formed (arrow). (G,H) Parallel cultures of heterozygous cells incubated with an EphA7 antibody exhibited marked reductions in cell attachment, aggregation, and chondrogenic nodule formation (arrow). (I) Incubation of homozygous mutant cultures with the same concentration of EphA7 antibody had only a minimal affect on the adhesion and condensation properties of these mutant cells. Scale bar: 50 μm.

umbilical arteries revealed a high level of Hoxa13^{GFP} expression in the condensing mesenchyme and differentiating endothelial layers (Fig. 2E,G,H). At higher magnification, cells forming the vascular wall appear highly disorganized in *Hoxa13*^{GFP} mutant homozygotes (Fig. 2H). Indeed, the stratification of vascular mesenchyme and endothelium was absent in mutants, whereas heterozygous littermate controls demonstrated normal mesenchymal and endothelial layer formation (Fig. 2G).

Immunohistochemical examination of proteins involved in vasculogenesis revealed a significant reduction in *EphA4* and *EphA7* expression in the condensing vascular mesenchyme and endothelium of *Hoxa13*^{GFP} mutant homozygotes (Fig. 9). These data demonstrate the levels of *EphA4* and *EphA7* expression are reduced in the mutant tissue, and again that the abnormal cellular organization of the mesenchyme and endothelium that form these vessels. It is important to note the changes in morphology exhibited in the mutant umbilical arteries does not create a generalized reduction in UA marker expression as even the ligand for *EphA4* and *EphA7*, *ephrin A3*, is normally expressed in the mutant vessels (Fig. 2H, inset). Interestingly, both EphA4 and EphA7 are still expressed normally in the gut, ventral neural tube and dorsal root ganglia in these same mutant homozygous embryos (data not shown).

DISCUSSION

Cell sorting, adhesion and aggregation represent some of the earliest stages in patterning undifferentiated mesenchyme (Takeichi, 1991; Gumbiner, 1996). During formation of the limb bones, this follows a stereotypic progression of condensation, branching and segmentation generating a pattern of prechondrogenic condensations, which subsequently give rise to each of the bony elements (Shubin and Alberch, 1986). In *Hoxa13*^{GFP} mutant homozygotes, the condensations needed

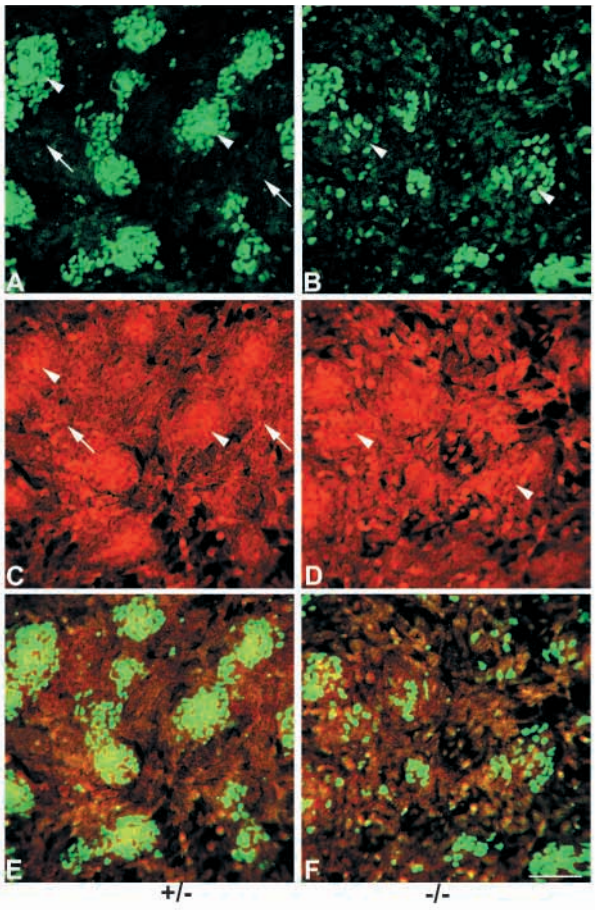

Fig. 7. Proximal-distal cell sorting of wild-type and *Hoxa13*^{GFP} limb mesenchyme. (A) Combinations of proximal wild-type and distal heterozygous mesenchyme cells 19 hours after inoculation. Note the sorting of heterozygous and wild-type mesenchyme cells into proximal (arrows) and distal (arrowheads) mesenchyme cell condensations. (B) Combinations of proximal wild-type and distal mutant mesenchyme cells 19 hours after inoculation. Note the inclusion of mutant cells into the wild-type condensations (arrowheads). (C) TO-PRO-3 iodide staining of wild-type and heterozygous mesenchyme cell condensations showing separation of proximal (arrows) and distal (arrowheads) condensations. (D) TO-PRO-3 iodide staining of proximal wild-type and distal mutant cells showing inclusion of mutant cells into proximal condensations (arrowheads). (E) Multiwavelength analysis showing sorting of distal heterozygous cells (green) from proximal wild-type cells (red). (F) Multiwavelength analysis showing a lack of sorting between distal mutant cells (green) and wild-type proximal cells (red). Scale bar: 100 μm.

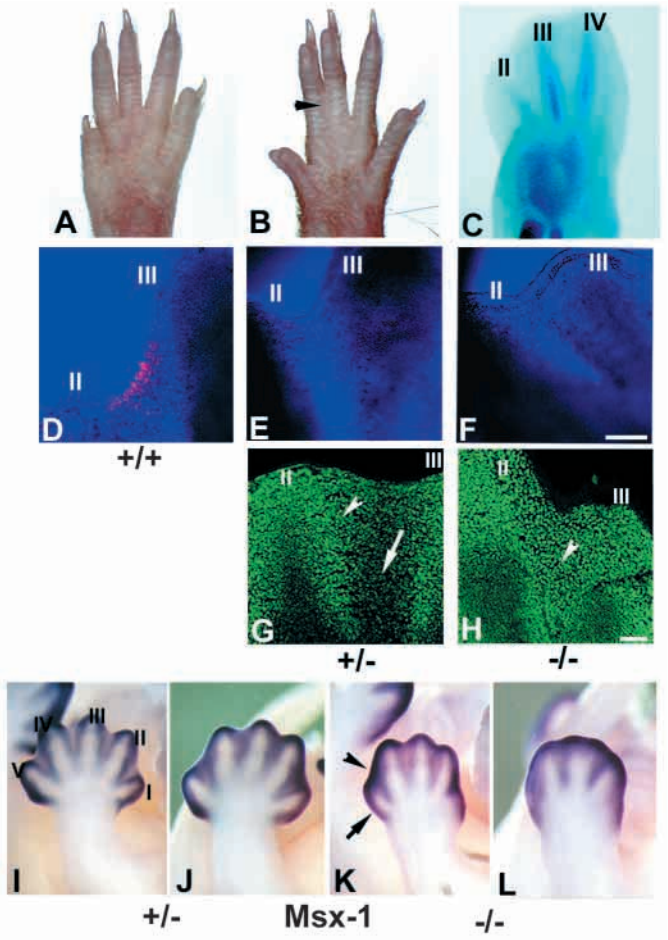

Fig. 8. Characterization of Msx-1 expression and interdigital apoptosis in limbs heterozygous and homozygous for the Hoxa13^{GFP} mutation. (A) Normal digit separation in wild-type adult hindlimb. (B) Digit II-III fusion (arrowhead) in a heterozygous adult hindlimb. (C) E13.5 mutant hindlimb showing no initiation of digit separation. (D) TUNEL assay of apoptosis between digits II and III in a wild-type E13.5 hindlimb. (E) Reduced apoptosis between digits II and III in a heterozygous hindlimb. (F) Absence of apoptosis between digits II and III in a mutant homozygous hindlimb. (G) Cryosections of a normally developing E 13.5 heterozygous hindlimb reveal low levels of ectopic interdigital cells (arrowhead) that express Hoxa13, as well as predominantly normal regression of GFP-expressing cells to the condensing digit mesenchyme (arrow). (H) Cryosections of homozygous Hoxa13^{GFP} mutant hindlimbs reveal a persistence of cells (arrowhead) in the interdigital regions, reflecting a failure of these cells to sort from the interdigital zone to the condensing digit mesenchyme. (I,J) Forelimb and hindlimb expression of Msx-1 in the interdigital tissues in a Hoxa13^{GFP} heterozygous embryo. (K,L) Forelimb and hindlimb expression of Msx-1 in homozygous mutant embryos. (K) Arrowhead indicates the interdigital region between digits IV and V where consistently higher levels of Msx-1 expression were detected in mutant forelimbs. By contrast, consistently lower levels of Msx-1 expression were also detected in mutant forelimbs in the posterior margin of digit V (arrow). Scale bars: 100 μm.

to form the entire first digit of the fore- and hindlimbs are absent, and the prechondrogenic condensations needed to form carpal, metacarpal, tarsal and metatarsal bones are not resolved. The residual capacity to form some of the autopod condensations in the *Hoxa13*^{GFP} mutant homozygotes is explained by the compensating expression of *Hoxd13*, as in embryos homozygous mutant for both genes, no autopod condensations are formed (Fromental-Ramain et al., 1996).

We have shown that *Hoxa13*^{GFP}-expressing cells, which lack functional Hoxa13 protein, are unable to attach efficiently to culture dishes and to form large condensates. They remain detached, cease to divide and die after a few days in culture. By contrast, *Hoxa13*^{GFP}-expressing cells that retain *Hoxa13* function (i.e. are heterozygous for the *Hoxa13* mutation) form robust prechondrogenic condensations, which in culture progress along the chondrogenic differentiation pathway.

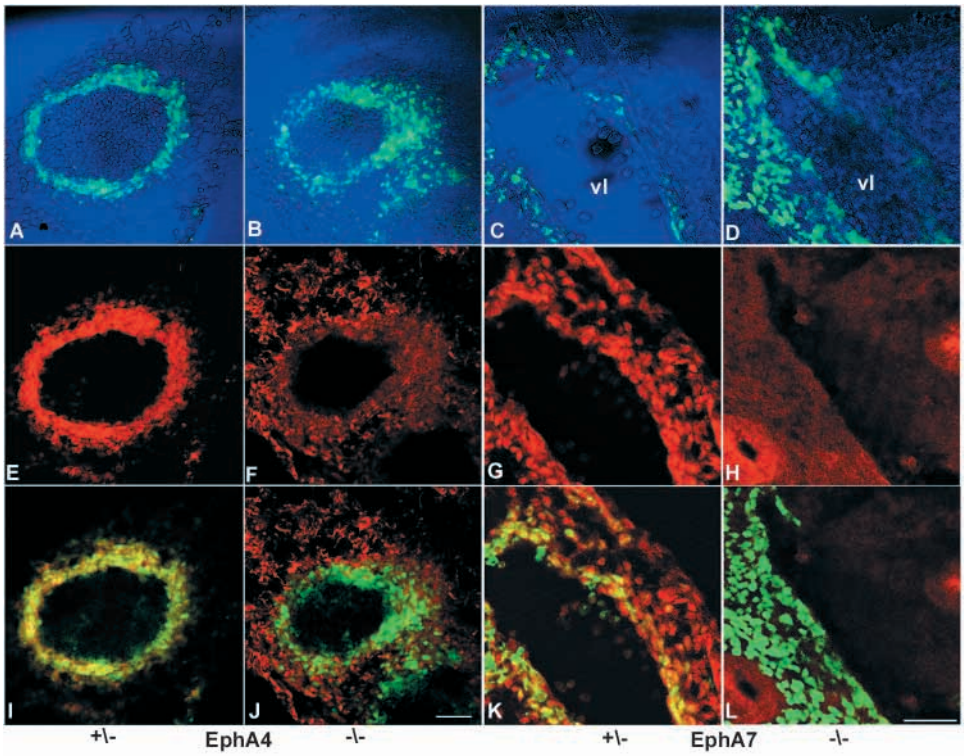

Fig. 9. EphA4 and EphA7 expression in the umbilical arteries (UAs) of E11.5 *Hoxa13*^{GFP} heterozygous and mutant homozygous littermates. (A,B) Hoxa13^{GFP} expression in the developing vascular wall of heterozygous and mutant homozygous embryos. (C,D) Hoxa13^{GFP} expression in the developing vascular wall of heterozygous and mutant embryos, vascular lumen (vl). (E) Expression of EphA4 in the developing UA vascular wall of heterozygotes. (F) Loss of EphA4 expression in the developing UA vascular wall of mutant homozygotes. (G) Expression of EphA7 in the developing wall of the UA of heterozygotes. (H) Loss of EphA7 expression in the developing wall of the UA in *Hoxa13*^{GFP} mutant homozygotes. (I) Multiwavelength analysis detects coexpression of EphA4 and Hoxa13^{GFP} in same cells within the developing UA walls of heterozygotes. (J) Multiwavelength analysis from a mutant homozygote UA demonstrates a loss of EphA4 expression in cells expressing Hoxa13^{GFP}. (K) Multiwavelength analysis of EphA7 and Hoxa13^{GFP} expression reveals co-expression in the cells of the developing UA wall in heterozygotes. (L) Multiwavelength analysis of a mutant homozygote reveals a loss of EphA7 expression in cells that express Hoxa13^{GFP} in the developing UA wall. Scale bar: 50 μm.

Hoxa13^{GFP}-null mesenchymal cells can form mixed prechondrogenic condensates with wild-type mesenchymal cells and then undergo chondrogenic differentiation. However, when *Hoxa13*^{GFP}-null cells are plated in the presence of wild-type mesenchymal cells isolated from a more proximal region of the limb bud, they do not sort themselves from the proximal cells. Thus, *Hoxa13* may regulate genetic pathways that control the adhesive properties of the distal limb mesenchyme and in the process, confer positional value along the proximodistal axis to this population of cells. Previous studies in chick (Yokouchi et al., 1995) support this conclusion, as misexpression of *Hoxa13* in the proximal limb bud alters proximal mesenchymal cell identity in the opposite manner, appearing to confer more distal limb character onto cells that normally do not express *Hoxa13*.

Alterations in the expression of *EphA7* and its ligand may explain the aberrant cell adhesion, sorting and boundary formation of the distal autopodal mesenchyme

In the condensing digit mesenchyme, *EphA7* expression closely parallels the expression of *Hoxa13*^{GFP}. At E11.5 both *Hoxa13*^{GFP} and *EphA7* are expressed strongly throughout the dorsal mesenchyme (this work; Araujo et al., 1998). By E13.5, the expression of *Hoxa13*^{GFP} and *EphA7* remains coincident in the perichondrium of the condensing forelimb digits. Interestingly, *ephrin A3* expression also overlaps with *Hoxa13*^{GFP} and *EphA7* in both E11.5 and E13.5 limbs, with expression finally restricted to the perichondrial region (Fig. 5C). This co-localization suggests a role for *Hoxa13* in mediating perichondrial boundary formation by positively regulating *EphA7* expression, which in turn interacts with *ephrin A3* to delineate the perichondrial boundary. The Eph receptors and their membrane-bound ligands are ideally suited to establish such boundaries, as their interactions provide the repulsive signals necessary to restrict intermingling between heterogeneous mesenchymal cell populations (Ciossek et al., 1995; Valenzuela et al., 1995; Wada et al., 1998). A similar role for this interaction may be evident in the reinforcement of the boundaries between rhombomeres of the vertebrate hindbrain (Taneja, 1996; Mellitzer et al., 1999; Xu et al., 1999).

In the autopod, reduced *EphA7* expression in conjunction with alterations in the expression of *ephrin A3* provides a molecular mechanism to explain both aberrant cell adhesion and defects in limb patterning associated with loss of *Hoxa13* function. In the distal limb, differential cell sorting is required to organize the undifferentiated mesenchyme into morphologically distinct musculoskeletal domains. Finally, antibody blocking of *EphA7* demonstrates that this receptor has the capacity to regulate autopod mesenchymal cell aggregation and chondrogenic nodule formation in vitro, providing a mechanistic link between the regions affected by loss of Hoxa13 function and the reduction of *EphA7* expression.

Because Hox genes have the capacity to regulate genes at multiple levels of a developmental cascade (Weatherbee et al., 1998), it is possible that other pro-adhesion molecules involved in autopod patterning are regulated by *Hoxa13*. Although we did not see a reduction in *EphA4* expression in the mutant autopod, other EphA family members may be involved in this process. The residual capacity of homozygous mutant cells to attach and form some chondrogenic nodules, as well as our observation that *EphA7* expression is not completely lost in

intact *Hoxa13*^{GFP} homozygous mutant embryos, leaves open the possibility that additional proteins, such as Hoxd13, function in parallel with Hoxa13 to pattern the autopod. Finally, our observation that *EphA7* expression is reduced in homozygous mutant limbs may suggest an indirect role for Hoxa13 in mediating EphA7 expression. However, our in vitro characterization of *EphA7* expression in FACS-enriched homozygous mutant cells, indicates that EphA7 expression is absent. This finding, in conjunction with normal levels of Msx-1 expression in intact mutant limbs, suggests that changes in EphA7 expression in the mutant autopod are more likely the result of direct regulation in specific tissues.

Limb defects in *Hoxa13*^{GFP} mutants: the role of programmed cell death

TUNEL assays of homozygous mutant limbs at E11.5 and 12.5 did not reveal significant increases in programmed cell death relative to control embryos (data not shown) which indicates that the reduced capacity to form the appropriate autopod prechondrogenic condensations observed in *Hoxa13* mutant homozygotes is not explained by increased apoptosis. On the contrary, this study revealed a loss of normal apoptosis in the interdigital regions of the autopod in *Hoxa13* mutant homozygotes and reduced apoptosis between digits II and III of embryos heterozygous for the *Hoxa13* mutation. The reduced level of apoptosis provides an explanation for the persistence of interdigital tissue in heterozygous and homozygous *Hoxa13* mutants. Normally, *Hoxa13* expression becomes restricted to the digit perichondrium by E13.5. However, in both heterozygous and homozygous *Hoxa13* mutant embryos, Hoxa13-GFP labeled cells are observed in the interdigital tissue (Fig. 7G,H). This observation provides another example of the reduced ability of *Hoxa13* mutant cells to sort themselves properly, resulting in the failure to establish an appropriate boundary between *Hoxa13*-expressing and nonexpressing tissues. The reduction or absence of normal apoptosis in the interdigital region of these mutant embryos might in turn follow from a failure of the ectopic *Hoxa13*-expressing cells to respond to apoptotic signals. Alternatively, the persistence of interdigital tissues could also result from changes in cell proliferation. An examination of mitotic cells in interdigital tissue using a mitosis-specific marker, anti-phosphohistone H3, did not reveal differences in the number of mitotic cells (data not shown).

Loss of *EphA4* and *EphA7* expression in the umbilical vasculature of *Hoxa13*^{GFP} mutants

The high level of *Hoxa13* expression in the condensing mesenchyme and endothelial layer of the UA suggests a major role for *Hoxa13* in the formation of these vessels. Narrowing of the UA is observed as early as E10.5 in *Hoxa13*^{GFP} homozygous embryos, with complete unilateral closure being seen in all of the E13.5 embryos examined. It is important to note that during murine gestation, the exiting UAs fuse into a single vessel outside the embryo proper (Kaufman and Bard, 1999), whereas humans typically maintain two UAs during gestation. This difference might explain why stenosis of a single UA may not be life threatening in midgestation to humans (Pavlopoulos et al., 1998), whereas stenosis of the UA in mice would severely impact the volume of blood that reaches the placenta in mice, particularly if the occlusion occurred proximal to or outside of the umbilical ring.

Analysis of the vessel walls of E13.5 embryos reveals distinct mesenchymal and endothelial cell types in heterozygous and wildtype littermates. The UA walls of *Hoxa13* mutant homozygotes, on the other hand, are disorganized with no stratification into morphologically distinct cell types. The loss of *EphA4* and *EphA7* expression in the developing UA wall of *Hoxa13* mutant homozygotes by E11.5 may well explain the loss of cellular organization in the formation and maintenance of the boundaries between vascular mesenchyme and endothelium. Numerous studies have suggested the interaction of ephrins and their receptors during vasculogenesis and angiogenesis (Pandey et al., 1995; McBride and Ruiz, 1998; Wang et al., 1998; Adams et al., 1999, Ogawa et al., 2000).

In summary, a prominent feature common to both the limb and umbilical artery defects observed in *Hoxa13* mutant homozygous embryos is a failure to organize and properly pattern the mesenchyme within these developing tissues. We have provided evidence that mesenchymal dysfunction, in part, be understood as defects in mesenchymal cell aggregation and adhesion. A loss of ephrin receptor expression was common to both tissues. These observations suggest that *Hoxa13* directly or indirectly controls the aggregation, adhesion and sorting capacity of the mesenchymal cells within the autopod in part by regulating the ephrin/Ephrin receptor signaling system. Modulation of this signaling system would ensure that the appropriate cellular boundaries are formed and maintained during morphogenesis of these tissues. This role of *Hoxa13*, though not necessarily its only role in the formation of the distal limb skeletal elements and umbilical vasculature, nevertheless begins to explain many of the cellular defects observed in these mutant animals.

We thank M. Allen, S. Barnett, C. Lenz, G. Peterson, K. Lustig, S. Nguyen and V. Scott for expert technical assistance. In addition, we thank Rebecca Reiter for helpful suggestions regarding the establishment of the *Hoxa13*^{GFP} micromass cultures as well as L. Oswald for help in preparation of this manuscript. Part of this research was supported by grants to HSS from the March of Dimes (Basil O'Connor Award) and the NIH (1R01DK59150-01).

REFERENCES

Adams, R. H., Wilkinson, G. A., Weiss, C., Diella, F., Gale, N. W., Deutsch, U., Risau, W. and Klein, R. (1999). Roles of ephrinB ligands and EphB receptors in cardiovascular development: demarcation of arterial/venous domains, vascular morphogenesis, and sprouting angiogenesis. *Genes Dev.* **13**, 295-306.

Ahrens, P. B, Solursh, M. and Reiter, R. (1977). Stage-related capacity for limb chondrogenesis in cell culture. *Dev. Biol.* **60**, 69-82.

Araujo, M., Piedra, M. E., Herrera, M. T., Ros, M. A. and Nieto, M. A. (1998). The expression and regulation of chick EphA7 suggests roles in limb patterning and innervation. *Development* **125**, 4195-4204.

Capecchi, M. R. (1994). Targeted gene replacement. *Sci. Am.* **270**, 54-61.

Chen, J. and Ruley, H. E. (1998) An enhancer element in the EphA2 (Eck) gene sufficient for rhombomere-specific expression is activated by HOXA1 and HOXB1 homeobox proteins. *J. Biol. Chem.* **273**, 24670-24765.

Ciossek, T., Millauer, B. and Ulrich, A. (1995). Identification of alternatively spliced mRNAs encoding variants of MDK1, a novel receptor tyrosine kinase expressed in murine nervous system. *Oncogene* **9**, 97-108.

Davis, A. P. and Capecchi, M. R. (1994). Axial homeosis and appendicular skeleton defects in mice with targeted disruption of *hoxd-11*. *Development* **120**, 2187-2198.

Davis, A. P., Witte, D. P., Hsieh-Li, H. M., Potter, S. S. and Capecchi, M.

R. (1995). Absence of radius and ulna in mice lacking Hoxa-11 and Hoxd-11. *Nature* **375**, 791-795.

Dollé, P., Dierich, A., LeMeur, M., Schimmang, T., Schuhbaur, B., Chambon, P. and Duboule, D. (1993). Disruption of the Hoxd-13 gene induces localized heterochrony leading to mice with neotenic limbs. *Cell* **75**, 431-441.

Dottori, M., Hartley, L., Galea, M., Paxinos, G., Polizzotto, M., Kilpatrick, T., Bartlett, P. F., Murphy, M., Köntgen, G. and Boyd, A. (1998). EphA4 (Sek1) receptor tyrosine kinase is required for the development of the corticospinal tract. *Proc. Natl. Acad. Sci. USA* **95**, 13248-13253.

Flenniken, A. M., Nicholas, W. G., Yancopoulos, G. D. and Wilkinson, D. G. (1996). Distinct and overlapping expression patterns of ligands for Eph-related receptor tyrosine kinases during mouse embryogenesis. *Dev. Biol*. **179**, 382-401.

Fromental-Ramain, C., Warot, X., Messadecq, N. . LeMeur, M., Dollé, P. and Chambon, P. (1996). Hoxa-13 and Hoxd-13 play a crucial role in the patterning of the limb autopod. *Development* **122**, 2997-3011.

Ganan, Y., Macias, D., Basco, R. D., Merino, R. and Hurle, J. M. (1998). Morphological diversity of the avian foot is related with the pattern of msx gene expression in the developing autopod. *Dev. Biol*. **196**, 33-41.

Godwin, A. R., Stadler, H. S., Nakamura, K. and Capecchi, M. R. (1998). Detection of targeted GFP-*Hox* gene fusions during mouse embryogenesis. *Proc. Natl. Acad. Sci. USA* **95**,13042-13047.

Gumbiner, B. M. (1996). Cell adhesion: The molecular basis of tissue architecture and morphogenesis. *Cell* **84**, 345-357.

Haack, H. P. and Gruss, P. (1993). The establishment of murine *Hox-1* expression domains during patterning of the limb. *Dev. Biol*. **157**, 410-422.

Hall, B. K. and Miyake, T. (1992). The membranous skeleton: the role of cell condensations in vertebrate skeletogenesis. *Anat. Embryol*. **186**, 107-134.

Hall, B. K. and Miyake, T. (1995). Divide, accumulate, differentiate: cell condensations in skeletal development revisited. *Int. J. Dev. Biol*. **39**, 881-893.

Holmberg, J., Clarke, D. L. and Frisen, J. (2000). Regulation of repulsion versus adhesion by different splice forms of an Eph receptor. *Nature* **408**, 203-206.

Ide, H., Wada, N. and Uchyama, K. (1994). Sorting out of cells from different parts and stages of the chick limb bud. *Dev. Biol*. **162**, 71-76.

Janis, L. S., Cassidy, R. M. and Kromer, L. F. (1999). Ephrin-A binding and EphA receptor expression delineate the matrix compartment of the striatum. *J. Neurosci*. **19**, 4962-4971.

Kaufman, M. H. and Bard, J. B. L. (1999). Postimplantation extra-embryonic development. In *The Anatomical Basis of Mouse Development*, pp. 28-29. New York: Academic Press.

Kondo, T. and Duboule, D. (1999). Breaking colinearity in the mouse HoxD complex. *Cell* **97**, 407-417.

Maden, M., Graham, A., Gale, E., Rollinson, C. and Zile, M. (1997). Positional apoptosis during vertebrate CNS development in the absence of endogenous retinoids. *Development* **124**, 2799-2805.

Manley, N. R. and Capecchi, M. R. (1995). The role of Hoxa-3 in mouse thymus and thyroid development. *Development* **121**,1989-2003.

Mansour, S. L., Thomas, K. R. and Capecchi, M. R. (1988). Disruption of the proto-oncogene int-2 in mouse embryo-derived stem cells: a general strategy for targeting mutations to nonselectable genes. *Nature* **336**, 348-352.

McBride, J. L. and Ruiz, J. C. (1998). Ephrin-A1 is expressed at sites of vascular development in the mouse. *Mech. Dev*. **77**, 201-204.

Mellitzer, G., Xu, Q. and Wilkinson, D. G. (1999). Eph receptors and ephrins restrict cell intermingling and communication. *Nature* **400**, 77-80.

Nagy, A., Rossant, J., Nagy, R., Abarmow-Newerly, W. and Roder, J. C. (1993). Derivation of completely cell culture-derived mice from early-passage embryonic stem cells. *Proc. Natl. Acad. Sci. USA* **90**, 8424-8428.

Ogawa, K, Pasqualini, R., Lindberg, R. A., Kain, R., Freeman, A. L. and Pasquale, E. B. (2000). The ephrin-A1 ligand and its receptor EphA2 are expressed during tumor neovascularization. *Oncogene* **52**, 6043-6052.

Owens, E. M. and Solursh, M. (1982). Cell-cell interaction by mouse limb cells during in vitro chondrogenesis: analysis of the Brachypod mutation. *Dev. Biol*. **91**, 376-388.

Pandey, A., Shao, H., Marks, R. M., Polverini, P. J. and Dixit, V. M. (1995). Role of B61, the ligand for the Eck receptor tyrosine kinase, in TNFα-induced angiogenesis. *Science* **268**, 567-569.

Pavlopoulos, P. M., Konstantinidou, A. E., Agapitos, E., Christodoulou, C. N. and Davaris, P. (1998). Association of single umbilical artery with congenital malformations of vascular etiology. *Pediatr. Dev. Pathol*. **1**, 487-493.

Schwenk, F., Baron, U. and Rajewsky, K. (1995). A cre-transgenic mouse strain for the ubiquitous deletion of loxP-flanked gene segments including deletion in germ cells. *Nucleic Acids Res.* **23**, 5080-5081.

Shubin, N. H. and Alberch, P. (1986). A morphogenetic approach to the origin and basic organization of the tetrapod limb. *Evol. Biol*. **20**, 319-387.

Studer, M., Gavalas A., Marshall, H., Ariza McNaughton, L., Riji, F. M., Chambon, P. and Krumlauf, R. (1998). Genetic interactions between Hoxa1 and Hoxb1 reveal new roles in regulation of early hindbrain patterning. *Development* **125**, 1025-1036.

Takeichi, M. (1991). Cadherin cell adhesion receptors as a morphogenic regulator. *Science* **251**, 1451-1455.

Taneja, R., Thisse, B., Rijli, F. M., Thisse, C., Bouillet, P., Dollé, P. and Chambon, P. (1996). The expression pattern of the mouse receptor tyrosine kinase gene MDK1 is conserved through evolution and requires *Hoxa-2* for rhombomere-specific expression in mouse embryos. *Dev. Biol*. **77**, 397-412.

Valenzuela, D. M., Rojas, E., Griffiths, J. A., Compton, D. L., Gisser, M., Ip, N. Y., Goldfarb, M. and Yancopoulos, G. D. (1995). Identification of full-length and truncated forms of Ehk-3, a novel member of the Eph receptor tyrosine kinase family. *Oncogene* **10**, 1573-1580.

Wada, N., Kimura, I., Tanaka, H., Ide, H. and Nohno, T. (1998). Glycosylphosphatidylinositol-anchored cell surface proteins regulate position-specific cell affinity in the limb bud. *Dev. Biol*. **202**, 244-252.

Wanek, N., Muneoka, K., Holler-Dinsmore, G., Burton, R. and Bryant, S. V. (1989). A staging system for mouse limb development. *J. Exp. Zool*. **249**, 41-49.

Wang, H. U., Chen, Z.-F. and Anderson, D. J. (1998). Molecular distinction and angiogenic interaction between embryonic arteries and veins revealed by *ephrin-B2* and its receptor *Eph-B4*. *Cell* **93**, 741-753.

Warot, X., Fromental-Ramain, C., Fraulob, V., Chambon, P. and Dollé, P. (1997). Gene dosage-dependent effects of the *Hoxa-13* and *Hoxd-13* mutations on morphogenesis of the terminal parts of the digestive and urogenital tracts. *Development* **124**, 4781-4791.

Weatherbee, S. D., Halder, G., Hudson, K. J. and Carroll, S. (1998). Ultrabithorax regulates genes at several levels of the wing-patterning hierarchy to shpae the development of the Drosophila haltere. *Genes Dev.* **12**, 1474-1482.

Xu, Q., Mellitzer, G., Robinson, V. and Wilkinson, D. G. (1999). In vivo cell sorting in complementary segmental domains mediated by Eph receptors and ephrins. *Nature* **399**, 267-271.

Yokouchi, Y., Nakazato, S., Yamamoto M., Goto, Y., Kameda, T., Iba, H. and Kuroiwa, A. (1995). Misexpression of *Hoxa13* induces cartilage homeotic transformation and changes cell adhesiveness in chick limb buds. *Genes Dev*. **9**, 2509-2522.